THE L3 PLASTIC SCINTILLATING FIBRE SYSTEM

LUCAS TAYLOR
Department of Physics, Northeastern University
110 Forsyth Street, Boston, MA 02115, U.S.A.

ABSTRACT

The L3 Plastic Scintillating Fibre system is used to calibrate the central tracking chamber, by providing independent measurements of track positions in the bending plane. This paper describes the technical performance of the system in the 1990 and 1991 LEP runs, the calibration procedure, and the resulting performance of the L3 central tracker.

1. Introduction

The L3 detector [1] is one of four detectors operating at the Large Electron Positron (LEP) collider which has been running at $\sqrt{s} \approx M_Z$ since 1989. Figure 1 shows a perspective view of the L3 detector.

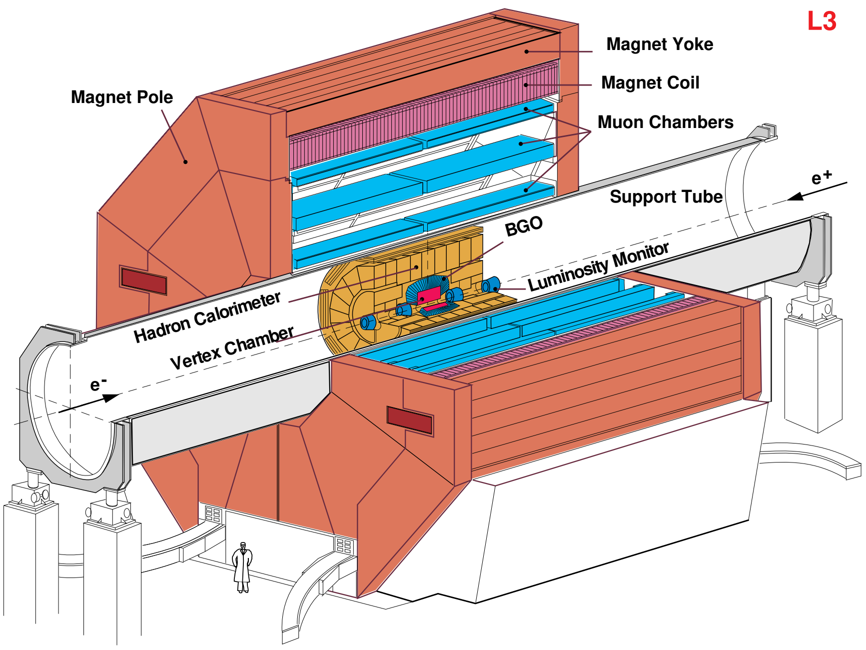

Figure 1: Perspective view of the L3 detector.

The relatively low magnetic field (0.5T) of the large conventional magnet and the small inner radius of the BGO electromagnetic calorimeter placed severe precision and size constraints on the L3 inner tracking chamber. A design was therefore chosen which used the time expansion principle. The segments of the Time Expansion Chamber [1, 2], or TEC, shown in figure 2, have a large drift region separated from a small amplification region. The low drift velocity (6μm/ns)

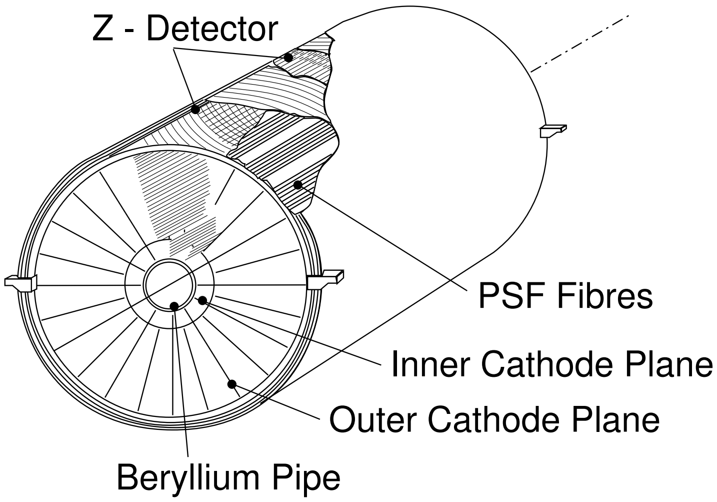

Figure 2: Perspective view of the TEC and PSF systems.

in the drift region enables a typical single hit resolution of 60μm to be obtained in the bending ($r\phi$) plane.

The Plastic Scintillating Fibre (PSF) system consists of a single layer of fibres mounted on the outside of the TEC, as shown in figure 2. Its purpose is to calibrate the TEC with sufficient precision to enable the high intrinsic accuracy of TEC to be fully exploited.

The following sections of this paper describe the TEC and PSF hardware configurations, the performance of the PSF system, and the PSF calibration method. Finally the performance of the TEC using the PSF calibration constants is presented, and compared to expectations and to results from a more conventional calibration method based on $Z \rightarrow \mu^+\mu^-$ events.

2. The Time Expansion Chamber

The TEC structure comprises a 1.5mm thick beryllium inner cylinder of radius 9.65mm and a 4.13mm thick aluminium outer cylinder of radius 456.75mm, closed at the ends by a pair of 40mm thick aluminium end-flanges with a 992mm inner separation. The TEC volume is divided into 12 inner and 24 outer sectors by planes of wires running parallel to the axes of the cylinders. Figure 3 shows the layout of one inner and two outer TEC sectors, projected into the $r\phi$ plane. Radially in the centre of each sector is a plane of anodes, 4.8mm apart, at a potential of 2.9kV. The inner and outer sectors have 8 and 54 anodes respectively. Between each pair of anodes, a focus wire at 2.1kV serves to reduce crosstalk and define the length of

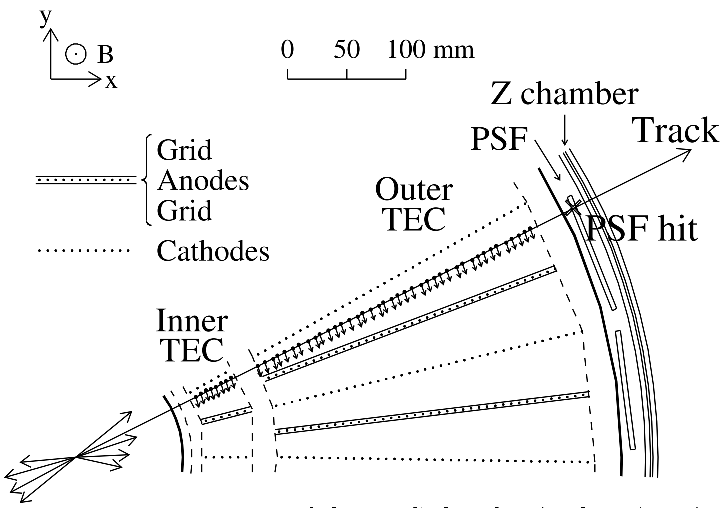

Figure 3: Two outer sectors of the TEC chamber in the $r\phi$ projection.

the track segment from which electrons reach each anode. At a distance of 3mm from (and parallel to) the anode plane is a grid plane of grounded wires. The space between the grid and anode wires, known as the drift-gap, is the region in which the gas amplification takes place. Radial cathode planes define the edges of the sector. The space between the cathode and grid planes is known as the drift region. The voltages of the cathodes increase with radius which, in conjunction with the field shaping wires at the other sector boundaries, ensures that the electric field in the drift region is almost uniform.

The TEC is filled with 80% CO_2 and 20% i–C_4H_{10} (isobutane). This gas mixture has low electron diffusion and a low drift-velocity ($\sim 6\mu$m/ns). A sophisticated slow-control system ensures that changes of the drift velocity in time (as a result of gas mixture, pressure and temperature variations) are less than 0.1%.

Due to an error in manufacture, some of the grid wires were not properly grounded, causing a distortion of the electric field in the drift region. Field distortions may also occur at the edges of the drift volumes despite the careful design of the field-shaping wire planes. Approximately 3% of the TEC anodes were rejected in the analyses described below, on the basis of an abnormal time distribution of hits, due to their being dead or subject to a grid or field-shaping problem.

3. The Plastic Scintillating Fibre system

For each of the 24 outer sectors, a PSF ribbon is mounted on the outside of TEC in a G10 holder at a radius of 459 mm, as shown in figures 2 and 3. Each ribbon is 1300 mm long $\times$ 101 mm wide $\times$ 1 mm thick and contains 143 fibres with 700 μm pitch, running parallel to the beam direction and covering 83% of the sector in azimuth. The scintillator has a polystyrene base doped with 1% butyl-PBD and

0.02% BDB and a spectral range of 300-500 nm. The fibres have an active width of 530μm and are surrounded by opaque cladding, to prevent crosstalk, and glued to the adjacent fibres. The manufacturer, namely The Kyowa Gas Company of Japan, has estimated that the position of the active fibre element fluctuates by no more than 35μm within any (fibre+cladding+glue) unit of width 700μm.

The ribbons are instrumented at one end only; the other end is mirrored to reduce light loss. On the readout side, the fibres are separated and threaded into two faceplates each having a 10×10 square array of holes, as shown schematically in figure 4. The two faceplates hold fibres 1-72 and 73-143, leaving 28 and 29

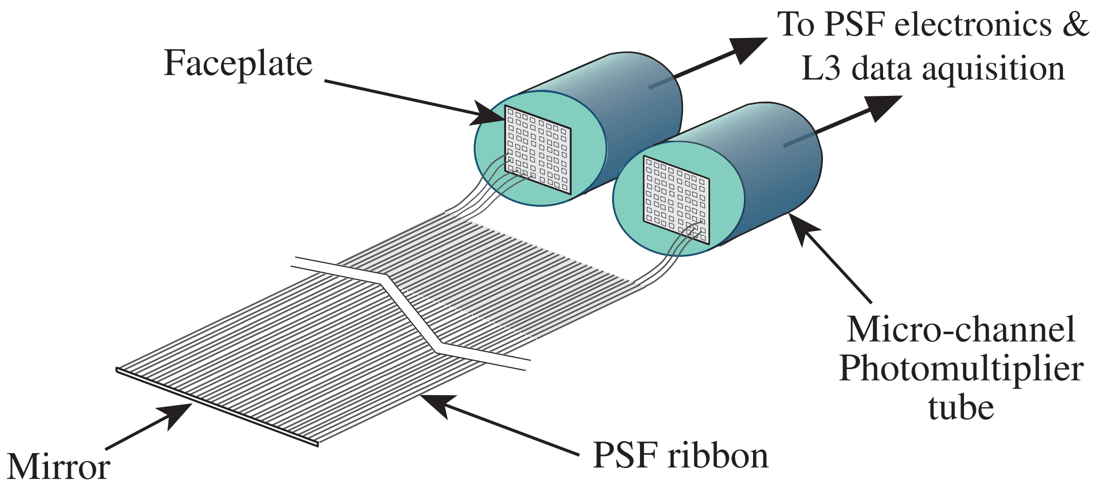

Figure 4: Schematic layout of one ribbon of the PSF system.

free holes respectively. Each faceplate is optically coupled to an ITT multi-anode micro-channel-plate (MCP) phototube. This interface must be carefully aligned to ensure the correct fibre-anode correspondence. The tube is read out, via a multiplex amplifier chip (MX4) and FADC, by the TEC readout system [2].

Figure 5 shows a typical pedestal spectrum for a single PSF channel, taken with beam and tube off. The pedestal values and corresponding sigmas for all channels of one tube are shown in figure 6. The average values and sigmas for the pedestals were the same within errors whether or not the tube was on. Mean pedestal values were in the range of 20-60 counts so signals saturate neither the MX4 amplifier nor the FADC. The r.m.s. of each pedestal distribution was typically less than 0.5 FADC counts, therefore thresholds of a few FADC counts were used. The PSF system was operated in digital readout mode, *i.e.* a single bit was set for each fibre according to whether or not the pedestal-subtracted pulse height exceeded the preset threshold. The PSF system is described in more detail in references 1–4.

4. Resolution and alignment

The PSF resolution is the accuracy with which the PSF can measure the position of a track in the $r\phi$ plane. It was measured by extrapolating TEC tracks

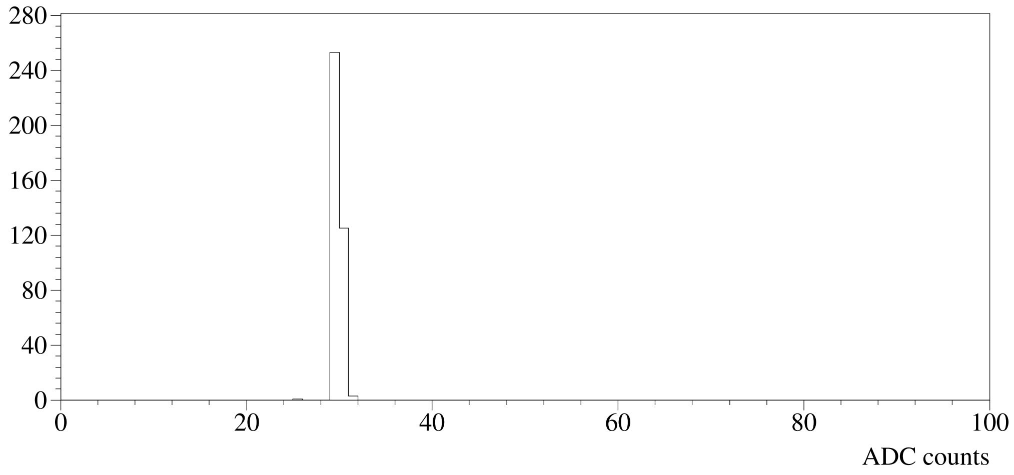

Figure 5: Typical pedestal spectrum for a single channel (beam and tube off).

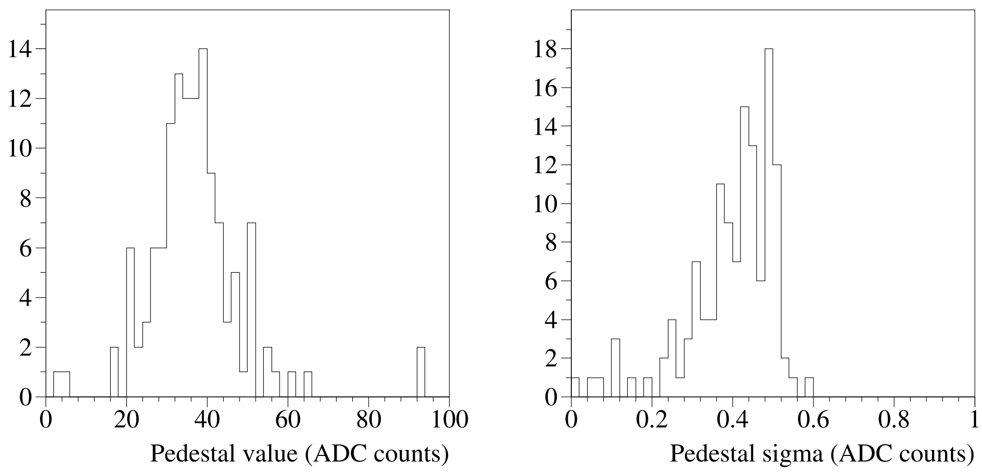

Figure 6: Pedestal values and sigmas for all channels of a typical tube (beam and tube off).

to the PSF ribbon and measuring the the $r\phi$ residual, ξ, defined as:

$$\xi = x_{\rm SF} - x_{\rm TK} \tag{1}$$

where $x_{\rm SF}$ is the distance of the hit fibre from the intersection of the extrapolated anode plane and the ribbon and $x_{\rm TK}$ is the distance from the anodes to the intersection point of the track with the ribbon. For perfect tracks and a perfect PSF system the residual distribution should be a square wave whose width corresponds to the active area of a single fibre. In reality, this ideal form is smeared by the errors on the TEC track extrapolation, random noise hits in the PSF and uncertainties in the PSF geometry. Figure 7 shows the residual distribution for a typical ribbon, using the corrected PSF geometry. The solid line is the result of a gaussian fit with

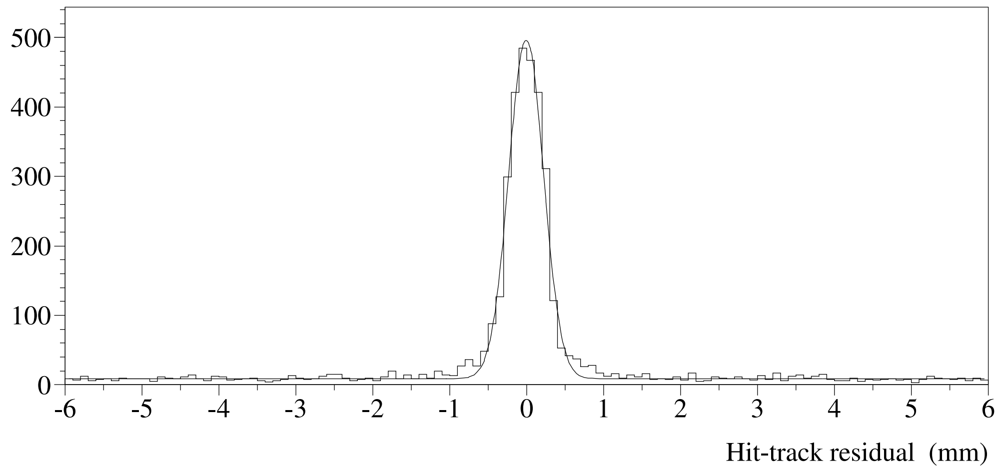

Figure 7: Track and PSF hit residuals for a typical PSF ribbon.

a flat background. The PSF resolution, defined as one standard deviation of the gaussian, is 245 μm averaged over all ribbons.

The alignment of the PSF ribbons was determined using TEC tracks, by requiring that the mean residuals were zero for each fibre of every ribbon. The radius and the slant of the ribbon with respect to the anode plane were determined to accuracies of 100 μm and 1 mrad respectively. The correlations of these quantities with drift velocity were small due to the use of both halves of the TEC sector and of tracks with a large curvature.

The azimuthal offset of the ribbon could not be measured independent of the TEC calibration and was therefore fixed to the nominal value. Similarly, the pitch of the fibres could not be measured using tracks since it is almost 100% correlated with the drift velocity. The pitch was therefore measured on a precision milling machine [5] to be 697$\pm$3 μm, where the the estimated error allows for measurement errors, differences between ribbons and (in a rough sense) for the possibility of occasional cracks in the cladding.

Variations of the PSF geometry due to temperature fluctuations are negligible due to the mechanical structure and the excellent stability of the temperature

($\pm 0.2°$). The variations in the geometry are Δ(Radius of PSF ribbon)$\sim 10\mu$m/°C and Δ(Width of PSF ribbon) $\sim 1\mu$m/°C.

5. Noise

Noisy PSF channels produce excessive numbers of hits which are *uncorrelated* to tracks. Although such occurrences can largely be removed by cutting on the hit and track matching residual, there is always a residual contamination of the data. Noisy channels were identified by plotting the total number of hits in each fibre which were *not* matched to the track within 3σ. Figure 8 shows the distribution of the number of unmatched hits per fibre for all the fibres of TEC. The distribution is

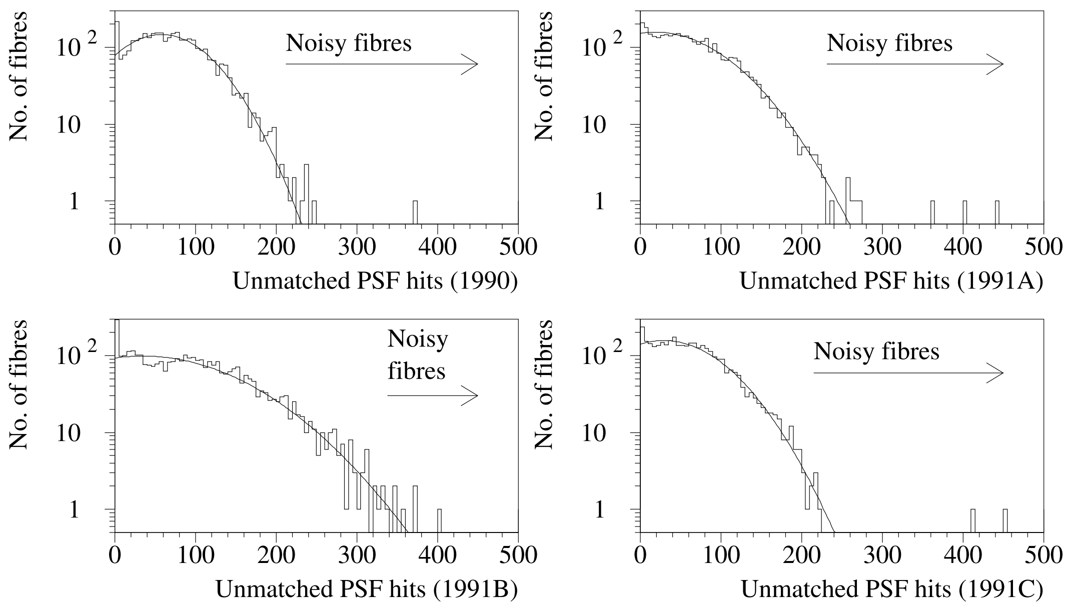

Figure 8: Number of unmatched hits per fibre.

fitted with a gaussian [1] and fibres falling more than three standard deviations from the mean were defined as too noisy and rejected in further analyses. This cut also rejects some good channels but their loss has a negligible effect on the efficiency. After rejection of noisy fibres the fraction of noise hits matched within 3σ to a track was typically 5%, corresponding to a signal to noise ratio of 20:1.

In addition to random noise hits, correlated hits in fibres adjacent to that through which the track passes were observed. This effect was studied using a sample with only one track in any particular half-sector. Given that a hit was found matched within 3σ to the track, the probability that there is an additional hit in an adjacent fibre was found to be 5%. This effect could be due to light leakage between fibres although measurements of similar fibres in the laboratory indicate

[1] There is no rigorous justification for the choice of a gaussian as the efficiencies vary from ribbon to ribbon. It does, however, describe the data well enough for these purposes.

that this is negligible. A GEANT simulation study of the TEC and PSF systems [6] concluded that δ-ray production in the material preceding the PSF gave a 5-15% probability for such correlated hits (the uncertainty is mainly due to an inadequate knowledge of the behaviour of the scintillator for different energy depositions).

For the drift velocity calibration only one hit is allowed to be matched to the track. If the genuine hit is lost due to the fibre inefficiency, however, it is possible for a noise or δ-ray hit to be associated to the track. On average this does not introduce a systematic bias. It does, however, degrade the PSF resolution slightly and hence increases the amount of data required to obtain a given calibration precision.

6. MCP tube and faceplate interface

If a fibre is threaded in the wrong faceplate hole, signals from this channel will be assigned to the wrong fibre number. By plotting the residual, ξ, as a function of the fibre number, misthreadings were easily identified by shifts in ξ by an integer multiple of the fibre pitch. Only six threading mistakes were found and these were corrected in the offline analysis.

If the MCP tube and the PSF faceplate are misaligned then light from a fibre may enter micro-channels corresponding to the wrong anode. The threading pattern of the faceplate is such that most vertically adjacent anode pairs are six fibres apart on the ribbon. For some tubes, a secondary peak was observed in the resolution plots which was displaced from the main peak by 4·2mm, corresponding to exactly six fibres. Figure 9 shows one such example observed. The misalignment

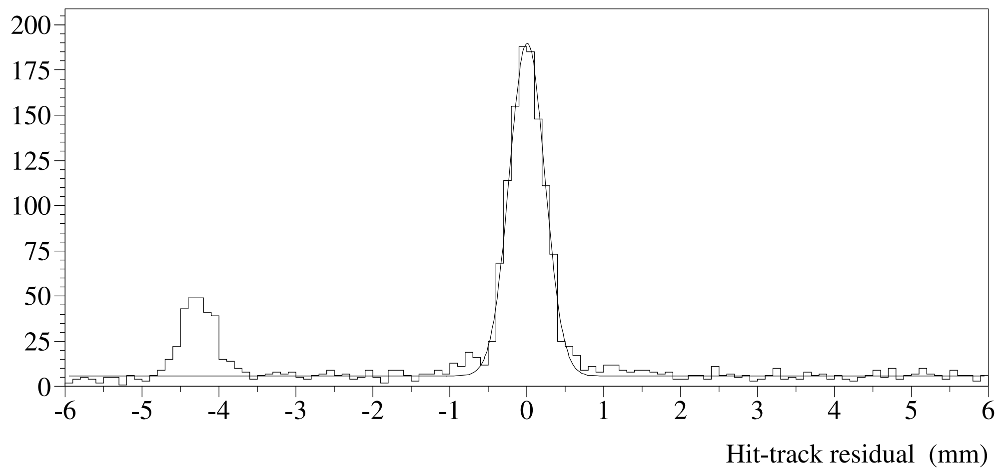

Figure 9: Secondary peak in the track-PSF hit residual distribution, indicating misalignment of the MCP tube and faceplate.

is caused by gravitational stress at the tube-faceplate interface. During the LEP shutdown after the 1990 run the tube-faceplate interface was modified to remove this problem and badly aligned tubes were re-aligned, such that since the start of the 1991 run only two minor cases of misalignment have been observed. Since hits in the second peak are rejected in all analyses the efficiency of misaligned tubes is reduced.

Optical grease was used at the interface of the tube and the faceplate to improve the optical coupling. Figure 10 shows the number of matched hits (proportional to the areas of the shaded boxes) for each fibre of two tubes, arranged according to the face-plate mapping. For the tube on the left, the number of hits

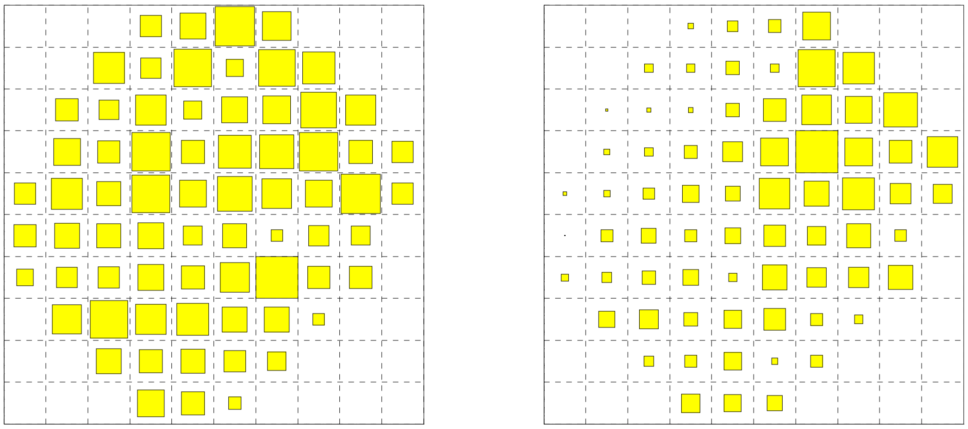

Figure 10: Number of matched PSF hits ($\propto$ size of shaded box) at tube–faceplate interface.

is approximately evenly distributed across the faceplate, apart from at the corners where there are no fibres. For the tube on the right, however, there is a strong dependence on position indicating poor optical coupling for certain regions of the interface. Examination of the tubes during the 1990/91 shutdown showed that such regions were caused by a lack of optical grease. This effect, seen for many tubes and particularly those on the upper half of TEC, tends to reduce the efficiency.

7. Efficiency

For a given integrated luminosity, the efficiency limits the statistical accuracy of the TEC drift velocities obtained from the PSF. Conversely, for a given accuracy, the efficiency determines the timescale required for a drift velocity calibration. The intrinsic PSF efficiency is defined as the probability that a track, passing through an *active* region of the PSF, will produce a PSF hit. The number of genuine PSF hits is obtained from a fit to the distribution of residuals, ξ, assuming a form :

$$n(\xi) = A + \frac{N_{\mathrm{Hits}}}{\sigma\sqrt{2\pi}} e^{-\xi^2/(2\sigma^2)} \tag{2}$$

where the constant term describes the flat background and N_{Hits} is the number of genuine PSF hits. The intrinsic PSF efficiency is given by:

$$\varepsilon = \frac{N_{\mathrm{Hits}}}{f_{\mathrm{s}}(1 - f_{\mathrm{d}} - f_{\mathrm{n}}) N_{\mathrm{Tracks}}} \tag{3}$$

where N_{Tracks} is the number of selected tracks which pass through the PSF ribbon, and f_{s}, f_{d} and f_{n} are defined as follows:

f_s = Fraction of each (fibre+cladding+glue) unit which is sensitive (75.8%).
f_d = Fraction of fibres which are dead.
f_n = Fraction of fibres which are noisy and hence rejected.

The average efficiency was 25% while the maximum efficiency obtained for any tube was 40%. No steady decrease of the efficiency with time, due to ageing of the MCP tubes or the fibres, has been observed.

The gain of the MCP tube is $\sim 10^6$ electrons/photoelectron and that of the charge-integrating MX4 amplifier is 0.7mV/fC. Thus one photoelectron yields a signal of ~112 mV or 14 FADC counts (1FADC count≡8 mV). This is consistent with the observed pulse height spectrum, as seen in figure 11 which shows the pedestal-subtracted pulse height spectrum for all fibres of a typical tube. The system yields

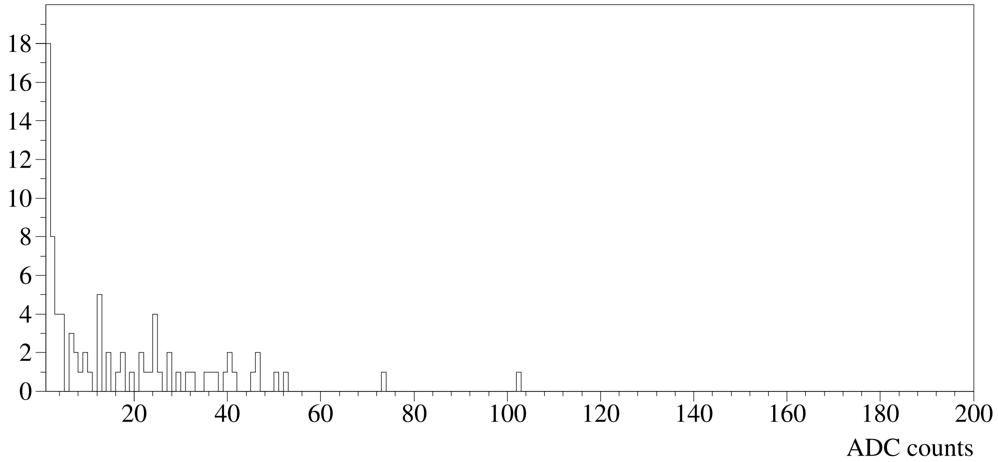

Figure 11: Pedestal-subtracted pulse height spectrum for a typical tube (beam and tube on).

typically ~0.4 photoelectrons which, assuming Poisson statistics, corresponds to an efficiency of ~33%. This is consistent with the measured average and maximum PSF efficiencies of 25% and 40% respectively.

8. Calibration of TEC using the PSF

The first step in the calibration of the drift region is to reconstruct tracks with a nominal set of calibration constants. For the drift region, a linear drift time-distance relation is assumed :

$$d = d_{\mathrm{grid}} + v_d(t - t_{\mathrm{grid}}) \tag{4}$$

where, v_d is the drift velocity (assumed constant), $t = t_{RAW} - t_0$, d_{grid} is the size of the drift gap, and t_{grid} is the t_0-corrected time corresponding to d_{grid}.

The definition of t_0 is the earliest time at which at genuine track can cause a hit on the anode. Due to deliberate electronics offsets this does not correspond to zero time but to approximately 100 ns, or 1% of the full time range. For each anode, t_0 was obtained by estimating the position of the leading edge of the drift-time distribution, obtained from ~100 000 tracks. This edge is not clearly defined due to limited statistics, noise, and reconstruction problems for tracks very close to the anodes. To evaluate t_0 for each wire with a reduced sensitivity to these problems, the cumulative integral of the drift-time distribution was used. The systematic error on t_0 was estimated to be 3ns.

Equation 4 may be written :

$$d = a + v_d t \qquad (\text{where} \;:\; a = d_{\text{grid}} - v_d t_{\text{grid}}) \tag{5}$$

Thus, the drift region calibration is described by two constants, a and v_d. The linearity assumption has been checked by comparing the position of the PSF hits with the predicted position from the extrapolation of the TEC track to the PSF ribbon, assuming a nominal set of *linear* calibration constants. As can be seen in figure 12, the relation is indeed highly linear. A similar study was carried out

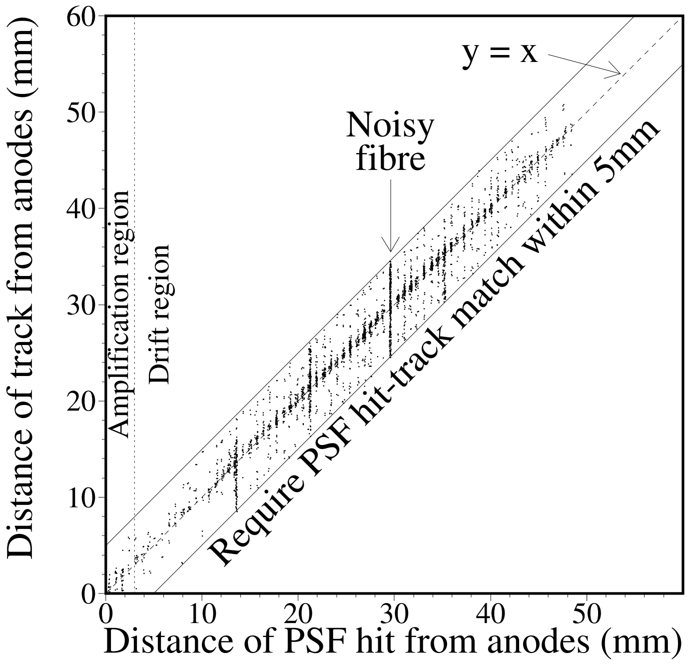

Figure 12: Perpendicular distances of track intersection points with PSF from the TEC anode plane, compared to the distance to the PSF hit.

comparing using elctron showers in the BGO calorimeter which confirmed linearity throughout the drift region of TEC.

All tracks from hadronic events with p_T >100MeV/c and with more than 30 outer TEC hits were used in the calibration of TEC. By exploiting the high statistics of the hadron sample [2] the constants a_i and $v_{d,i}$ could be obtained very precisely for

[2]Separate calibrations were performed for the 1990, 1991A, 1991B and 1991C data-taking periods with $\sim 10^5$

every single anode i. For each anode separate constants were obtained for the drift volumes on either side of the anode plane. The calibration algorithm consisted of the following steps:

1. All tracks are fitted assuming nominal calibration constants a_i^0 and $v_{d,i}^0$, the calculated t_0 values and the Lorentz angle of 2.4°obtained from the dimuon calibration. The measured beam centroid position [7] in the xy plane is included as an extra point in the fit with an error of $\sqrt{\sigma_x^2 \sin^2\phi + \sigma_y^2 \cos^2\phi}$. The RMS widths, σ_x and σ_y, of the beam have been measured with Bhabha events [7] independent of the event vertex position, to be $\sigma_x = 157\mu$m and $\sigma_y = 23\mu$m. The L3 track fitting routine is used and the residuals of the hits to the fitted track are calculated.

2. For each anode, a linear fit is made to the residual *vs.* drift-time plot over the region $t_{\rm grid} < t_d < 0.8t_{\rm cathode}$, where $t_{\rm cathode}$ is the drift time for a hit on the cathode plane. Ideally the residuals should be zero for all drift times with a spread given by the intrinsic TEC resolution. In practice these plots have an offset and slope which provide corrections, Δa_i^0 and $\Delta v_{d,i}^0$, to the assumed calibration constants a_i^0 and $v_{d,i}^0$.

3. For each outer TEC half-sector, a linear fit to the TEC-PSF residuals as a function of drift time gives a global correction to the drift velocity but *not* to the constant a due to the uncertainty in the azimuthal alignment of the PSF.

4. The single wire corrections, Δa_i^0 and $\Delta v_{d,i}^0$, and the half sector-by-half sector global drift velocity corrections are then applied to the nominal constants to obtain improved values, a_i^1 and $v_{d,i}^1$, for each anode.

5. Steps 1.-4. are then repeated using the improved constants, a_i^1 and $v_{d,i}^1$. Five iterations of this procedure are made after which the corrections to the calibration constants are negligible.

This method automatically matches the tracks inner and outer TEC track segments. It does not allow for inhomogeneities in the electric field close to the grid or field shapers since the drift velocity for each anode is assumed to a constant throughout the drift region.

Figure 13 shows the residual distributions for several TEC anodes with the dimuon calibration method and the PSF calibration method described above. The plots show examples of the four cases encountered – from top left to bottom right, anodes with: almost no problem, offset in a, incorrect v_d and non-linearity in the drift distance-time relation. In each example the PSF calibration algorithm improves the residual distribution.

Figure 14(upper) shows the variation of v_d with anode number for a typical good half sector. The drift velocity is approximately constant within the inner and outer sectors separately apart from close to the edges of the TEC. The PSF and dimuon calibrations are in good agreement, although the statistical errors on the PSF values are considerably smaller: $\sigma(v_d) \approx 0.1\%$ for each anode. The systematic

tracks/sector/calibration period.

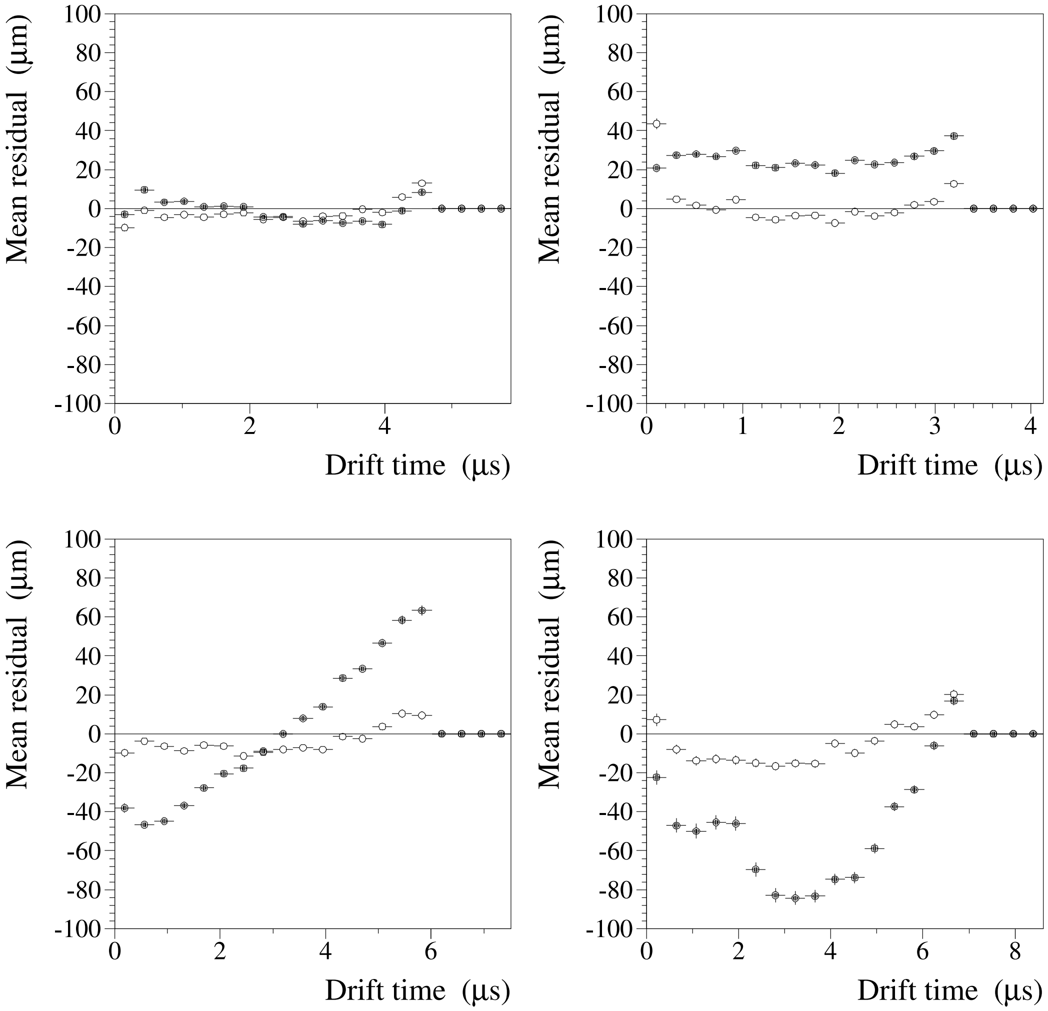

Figure 13: Single anode residual distributions for the dimuon calibration (filled circles) and the PSF calibration (open circles).

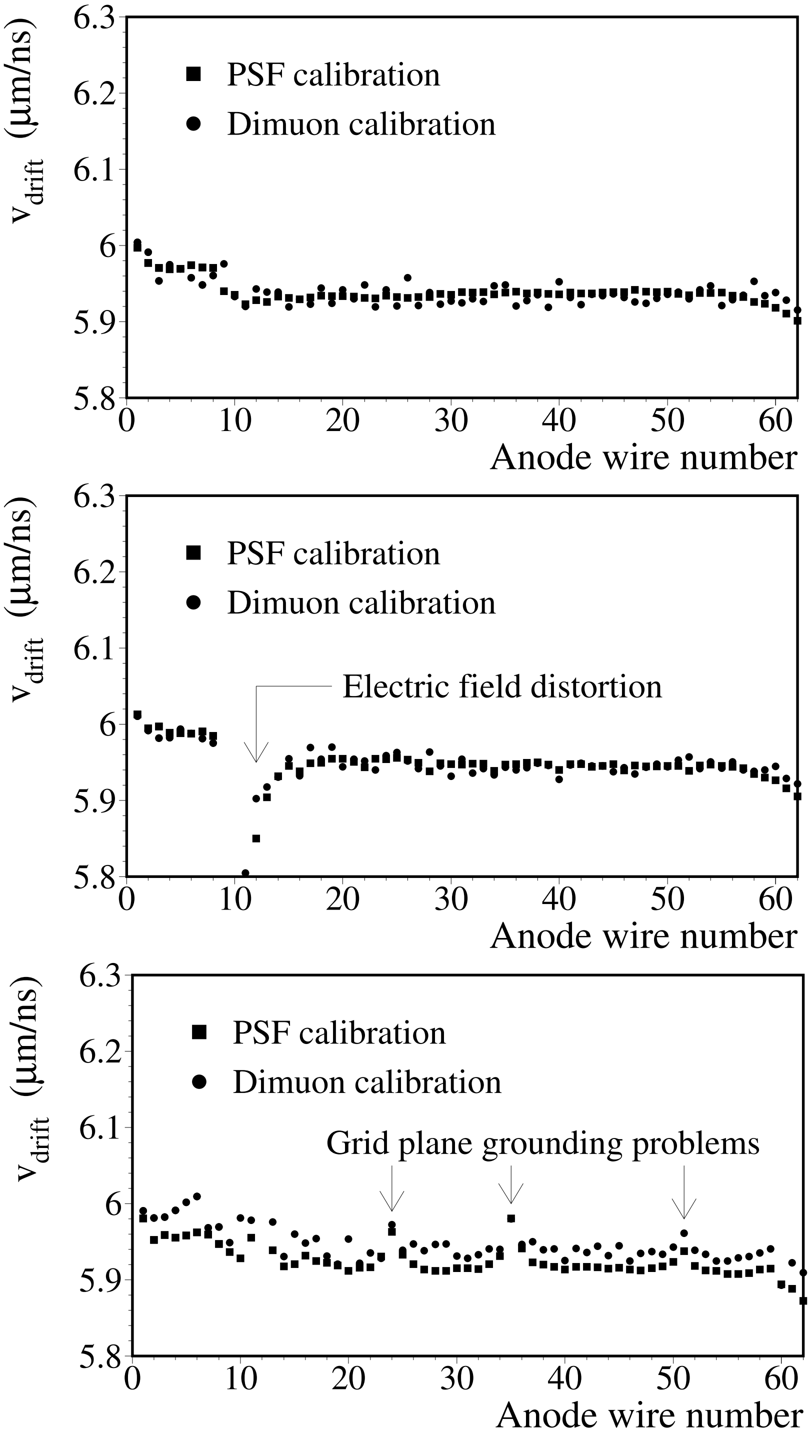

Figure 14: Drift velocity, v_d, as a function of anode number for a three half sectors of TEC, for the PSF (squares) and dimuon (circles) calibrations.

error on v_d is dominated by the uncertainty in the fibre pitch, and is estimated to be $\Delta v_d / v_d \approx 0.4\%$.

Figure 14(centre) shows the effect of an abnormal electric field distortion at the start of the outer TEC, while figure 14(lower) shows the effects of grid grounding problems close to pickup wires 24, 35 and 51. Although bad anodes are excluded in the track fits of the calibration algorithm, they are nonetheless calibrated as well as is possible within the linear assumption for the time-distance relation.

9. Single hit, momentum and impact parameter resolutions

The single wire resolution is measured from the spread of the residuals of the hits to the fitted tracks. For the residuals to be an unbiassed estimate of the resolution, the correct single wire resolution as a function of drift distance, $\sigma(d)$, must be used in the track fitting. Since the resolution is *a priori* unknown, an iterative method was used. Typically the resolutions obtained were 300–500μm inside the detection gap and 40μm just outside the detection gap. As the drift distance increases the resolution increases, due to diffusion in the gas, up to a maximum value of $\sim$100 μm close to the cathodes.

The impact parameter resolution was measured using Bhabha and dimuon events [7]. Since the leptons are produced at the same point and are almost back-to-back, the distance between the tracks near the origin is a convolution the impact parameter errors of the two tracks, independent of the beam spot position and size. The transverse momentum resolution was obtained from the dimuon sample by comparing the transverse momentum measured in TEC to that of the muon chambers (which have a resolution of $\Delta p/p$ =2.5% for $p \approx 45$ GeV/c).

The resolutions obtained with the dimuon and PSF calibration methods are summarised in table 1. The momentum and position constraints of the dimuon and

	Predicted	Dimuons	PSF
Impact parameter resolution (μm)	$\sim$105	$\sim$142	$\sim$109
$\sigma(1/p_{\mathrm{T}})$ (GeV^{-1})	$\sim$0.017	$\sim$0.023	$\sim$0.026

Table 1: Comparison of the impact parameter and transverse momentum resolutions, obtained using the dimuon and PSF calibration methods, with the predicted ideal values.

PSF calibration methods respectively are reflected in the values obtained for the momentum and impact parameter resolutions. Work is in progress to combine the two methods to simultaneously exploit the advantages of each method.

10. Conclusions

The performance of the L3 PSF system in the 1990 and 1991 LEP runs has been evaluated. The PSF resolution of 245μm and the signal to noise ratio of 20:1 are excellent. The average efficiency of 25% is sufficient for the required accuracy of the calibration constants. The PSF system has attained the design goal of 0.1% statistical errors on the TEC drift velocity such that the calibration is limited by the systematic error of 0.4% from the uncertainty in the fibre pitch.

Acknowledgements

I would like to thank all those people on L3 who have contributed to the PSF project, particularly those from ETH, Zürich, Johns Hopkins University, Baltimore, and Northeastern University, Boston who played a major role in the construction, maintenance and offline analysis of the PSF system. This work was supported in part by the National Science Foundation.

References

1. B. Adeva et al. "The construction of the L3 experiment." Nucl. Instr. and Meth. **A289** (1990) 35.
2. F. Beissel et al. "Construction and performance of the L3 central tracking detector." Nucl. Instr. and Meth. **A332** (1993) 33.
3. H. Akbari et al. "A readout system for plastic scintillating fibers." Nucl. Instr. and Meth. **A302** (1991) 415–426.
4. L. Taylor. "Performance of the L3 plastic scintillating fibre calibration system in the 1990 LEP run." L3 Note **883** (1991).
   G. Alverson, J. Bao, A. Gougas, I. Leedom, C. Spartiotis, and L. Taylor. "The Performance of the L3 plastic scintillating fibre calibration system in the 1990 and 1991 LEP runs." L3 Note **1105** (1992).
5. Private communication with M. MacDermott, ETH, Zürich and I. Leedom, Northeastern University, Boston.
6. G. Alverson. "Simulation of the behaviour of plastic scintillating fibres." L3 Note **931** (1991).
7. L. Taylor. "Measurements of the statistical and systematic errors of the TEC impact parameter and the size and position of the LEP beam spot." L3 Note **1480** (1993).